Journal of Sound and Vibration (1997) **207**(3), 335–350

FREE VIBRATION ANALYSIS OF MINDLIN PLATES WITH UNIFORM ELASTIC EDGE SUPPORT BY THE SUPERPOSITION METHOD

D. J. GORMAN

Department of Mechanical Engineering, University of Ottawa, 770 King Edward Avenue, Ottawa K1N 6N5, Canada

(*Received* 13 *November* 1996, *and in final form* 5 *May* 1997)

Utilizing the superposition method, a solution is obtained for the free vibration eigenvalues of Mindlin plates resting on uniform lateral elastic edge support. Subsequently, it is shown how minor modifications to the eigenvalue matrix permit the incorporation of the additional effects of rotational stiffness into the analysis. Solutions are based on the Mindlin thick plate theory. Convergence is rapid and eigenvalue curves are plotted for square plates and plates of aspect ratio 1·5, for various lateral and rotational spring stiffnesses. Digital results are tabulated in order that other analysts will have reliable data against which their findings may be compared.

1. INTRODUCTION

It is well known that while classical rectangular plate edge conditions, referred to as clamped and simply supported, are easy to formulate mathematically they are rarely fully achieved in actual practice. This is particularly true of clamped edge conditions, which are difficult to simulate experimentally, even under laboratory conditions.

For these and other reasons, a considerable amount of research effort has been devoted in recent years toward exploring the effects of elasticity in edge supports on rectangular plate free vibration frequencies. While it is not the intent here to present an exhaustive listing of all related publications a number of publications of immediate interest in the preparation of the present paper are noted. These include the early publication of Warburton and Edney [1], a more recent publication by Kim *et al*. [2], and a sequence of papers by the present author [3–6]. The first four references above pertain to problems where the elastic stiffness coefficients are constant (uniform) along any one edge. The latter two references are more general in that the stiffness coefficients may be made to take on any desired spacial distribution along any edge.

All of the above publications, and most other related publications, have one characteristic in common. They deal only with the free vibration of thin isotropic plates. An exception is the work of Saha *et al*. [7]. They have examined the effects of lateral and rotational elastic edge support on thick plates using an energy variational approach. Their handling of the problem is somewhat complicated since it involves utilizing products of Timoshenko beam solutions to represent the displacement and cross-sectional rotation functions. The method is further complicated by the fact that the beam functions are given rotational and lateral elastic support at each end.

The present paper begins by utilizing Mindlin thick plate theory and the superposition method to investigate the behaviour of plates resting on uniform lateral elastic edge

0022–460X/97/430335 + 16 $25.00/0/sv971107

support. Finally, it is shown how minor modifications to the eigenvalue matrix permits incorporation of the effects of edge rotational elastic support into the analysis. While attention is focused here on thick plates, it is also known that these effects cannot be neglected in the study of composite plates, even when they are thin. Composite plates resting on elastic supports will constitute the subject of a future paper.

The objective of this paper then, is to exploit the superposition method in analysing the free vibration behaviour of thick rectangular plates resting on uniform elastic edge support. Specifically, attention is initially focused on plates resting on uniform lateral elastic support. Subsequently, the effects of rotational elastic support along the edges are analysed and discussed.

2. MATHEMATICAL PROCEDURE

Accurate analytical type solutions to the problems of interest are obtained by means of the method of superposition. This method, which was exploited in references [3] through [6], involving thin plate theory, was also utilized in references [8] and [9] involving Mindlin theory. In view of the rather extensive description of the method as it applies to Mindlin theory, in reference [9], a further detailed description is not required here. A brief description will be provided only, for the sake of completeness.

2.1. FORCED VIBRATION SOLUTIONS SUPERIMPOSED

In the superposition technique a set of judiciously selected boundary driven harmonic forced vibration solutions (building blocks) are superimposed one-upon-the-other. In order to investigate the present problem of interest the set of building blocks represented schematically in Figure 1 are utilized. Slip-shear conditions are imposed along all non-driven edges. This condition is indicated by two small circles adjacent to the edges. Slip-shear conditions, as they relate to the Mindlin theory, imply a condition of zero transverse shear and zero torsional moment along the edge. They also imply a condition of zero rotation of the plate cross-section about an axis running along the edge at the plate mid-surface.

One begins by focusing attention on the first building block. It is driven by an imposed distributed harmonic transverse shear force of circular frequency ω. Two connected solid dots adjacent to the driven edge indicate that edge conditions differ from slip-shear conditions only in that the transverse shear force is not equal to zero.

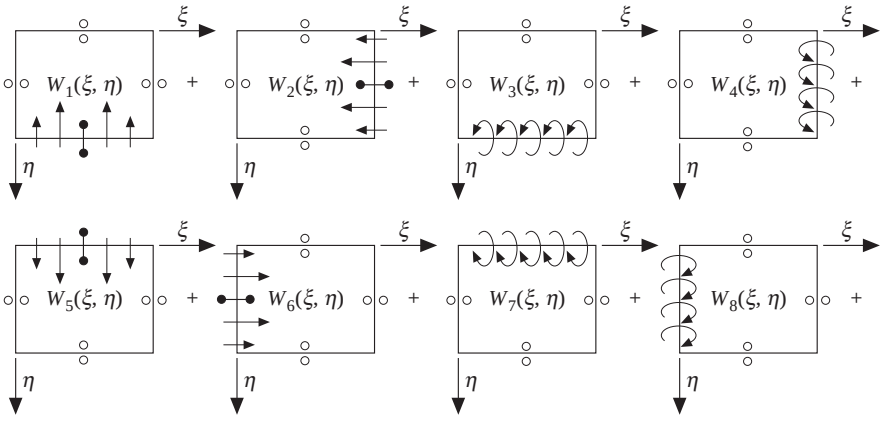

Figure 1. Schematic representation of building blocks utilized in theoretical analysis.

The spacial distribution of the imposed harmonic shear force is expressed in series form as

$$Q_\eta|_{\eta=1} = \sum_{m=1,2}^{K} E_m \cos(m-1)\pi\xi. \tag{1}$$

The governing differential equations based on the Mindlin theory are, in dimensionless form [9],

$$\frac{\partial^2 W}{\partial\xi^2} + \frac{1}{\phi^2}\frac{\partial^2 W}{\partial\eta^2} + \frac{\partial\psi_\xi}{\partial\xi} + \frac{1}{\phi}\frac{\partial\psi_\eta}{\partial\eta} + \frac{\lambda^4\phi_h^2}{v_3} W = 0, \tag{2}$$

$$\frac{\partial^2\psi_\xi}{\partial\xi^2} + \frac{v_1}{\phi^2}\frac{\partial^2\psi_\xi}{\partial\eta^2} + \frac{v_2}{\phi}\frac{\partial^2\psi_\eta}{\partial\xi\,\partial\eta} - \frac{v_3}{\phi_h^2}\left(\psi_\xi + \frac{\partial W}{\partial\xi}\right) + \frac{\lambda^4\phi_h^2}{12} W = 0, \tag{3}$$

$$\frac{\partial^2\psi_\eta}{\partial\xi^2} + \frac{1}{\phi^2 v_1}\frac{\partial^2\psi_\eta}{\partial\eta^2} + \frac{v_2}{\phi v_1}\frac{\partial^2\psi_\xi}{\partial\xi\,\partial\eta} - \frac{v_3}{\phi_h^2 v_1}\left(\psi_\eta + \frac{1}{\phi}\frac{\partial W}{\partial\eta}\right) + \frac{\lambda^4\phi_h^2}{12v_1}\psi_\eta = 0. \tag{4}$$

Transverse shear forces, bending moments, etc., are written as

$$Q_\xi = \psi_\xi + \partial W/\partial\xi, \qquad Q_\eta = \psi_\eta + (1/\phi)\,\partial W/\partial\eta, \qquad M_\xi = \partial\psi_\xi/\partial\xi + (v/\phi)\,\partial\psi_\eta/\partial\eta,$$
$$M_\eta = \partial\psi_\eta/\partial\eta + v\phi\,\partial\psi_\xi/\partial\xi, \qquad M_{\xi\eta} = \partial\psi_\eta/\partial\xi + (1/\phi)\,\partial\psi_\xi/\partial\eta. \tag{5}$$

When the first building block of Figure 1 is driven by the first term of equation (1) the problem will be one-dimensional in nature, i.e., the response will not be a function of the co-ordinate ξ. In this case the governing differential equations reduce to the following pair [9]:

$$\mathrm{d}^2 W/\mathrm{d}\eta^2 + \phi\,\mathrm{d}^2\psi_\eta/\mathrm{d}\eta^2 + \lambda^4\phi^2\phi_h^2 W/v_3 = 0 \tag{6}$$

and

$$\frac{\mathrm{d}^2\psi_\eta}{\mathrm{d}\eta^2} - (v_3\phi^2/\phi_h^2)\,(\psi_\eta + (1/\phi)\,(\mathrm{d}W/\mathrm{d}\eta)) + \lambda^4\phi^2\phi_h^2\psi_\eta/12 = 0. \tag{7}$$

One seeks now the response of the first building block to the first driving term. It is convenient to represent the plate lateral displacement and cross-section rotation ψ_η as

$$W(\eta) = X(\eta) \qquad \text{and} \qquad \psi_\eta(\eta) = Z(\eta).$$

The governing differential equations then take the form

$$X''(\eta) + a_{m1} Z'(\eta) + b_{m1} X(\eta) = 0 \tag{8}$$

and

$$Z''(\eta) + a_{m3} X'(\eta) + b_{m5} Z(\eta) = 0, \tag{9}$$

where superscipts imply differentiation with respect to η and the coefficients $a_{m1}\ldots$ etc., are defined in reference [9].

By applying the correct differential operators to this pair of equations, as was done in reference [9], the parameter $X(\eta)$ is eliminated and one is left with an ordinary fourth order homogeneous differential equation involving the parameter $Z(\eta)$. The roots associated with the corresponding characteristic equation are all real for the present range of interest [9]. Designating the three possible combinations of the pairs of associated roots

as R_1, R_2, one has three possible forms of solution,

$$\text{Case} = 1,\ R_1, R_2 < 0{\cdot}0; \quad \text{Case} = 2,\ R_1 < 0{\cdot}0;\ R_2 > 0{\cdot}0; \quad \text{Case} = 3,\ R_1, R_2 > 0{\cdot}0, \quad (10)$$

In all computations conducted in connection with the present paper only case 2 has been encountered. Recognizing that the functions $X(\eta)$ and $Z(\eta)$ must be symmetric and antisymmetric, respectively, with respect to the ξ-axis it follows that one may write, for case 2,

$$X(\eta) = A_m \cos \alpha\eta + B_m \cosh \beta\eta, \qquad Z(\eta) = A_m S_{m1} \sin \alpha\eta + B_m S_{m2} \sinh \beta\eta, \qquad (11, 12)$$

where $\alpha = \sqrt{|R_1|}$, and $\beta = \sqrt{|R_2|}$.

Expressions S_{m1} and S_{m2} are obtained by utilizing the coupling of equations (8) and (9), as was done in reference [9].

Finally, imposing the boundary conditions of $Q_\eta = E_m$ and $\psi_\eta = 0$, at $\eta = 1$, one obtains the response of the building block as

$$X(\eta) = (E_m/X2)\{\cos \alpha\eta + X1 \cosh \beta\eta\}, \qquad (13)$$

$$Z(\eta) = (E_m/X2)\{S_{m1} \sin \alpha\eta + X1 S_{m2} \sinh \beta\eta\}, \qquad (14)$$

where $X1$ and $X2$ are easily obtained.

One next examines the response of the first building block to driving terms with the subscript $m > 1$. The steps taken are described in detail in reference [9].

In view of the boundary conditions prescribed along the edges $\xi = 0$ and $\xi = 1$, Lévy type solutions for the parameters $W(\xi, \eta) \ldots$ etc., are written as

$$W(\xi, \eta) = X_m(\eta) \cos m\pi\xi, \qquad \psi_\xi(\xi, \eta) = Y_m(\eta) \sin m\pi\xi, \qquad \psi_\eta(\xi, \eta) = Z_m(\eta) \cos m\pi\xi. \qquad (15\text{–}17)$$

Substituting these expressions in the governing differential equations one obtains, for any $m > 1$, the following set of coupled ordinary homogenous differential equations. They are written in matrix form as

$$\begin{Bmatrix} X_m'' \\ Y_m'' \\ Z_m'' \end{Bmatrix} + \begin{bmatrix} 0 & 0 & a_{m1} \\ 0 & 0 & a_{m2} \\ a_{m3} & a_{m4} & 0 \end{bmatrix} \begin{Bmatrix} X_m' \\ Y_m' \\ Z_m' \end{Bmatrix} + \begin{bmatrix} b_{m1} & b_{m2} & 0 \\ b_{m3} & b_{m4} & 0 \\ 0 & 0 & b_{m5} \end{bmatrix} \begin{Bmatrix} X_m \\ Y_m \\ Z_m \end{Bmatrix} = \begin{Bmatrix} 0 \\ 0 \\ 0 \end{Bmatrix}, \qquad (18)$$

where the quantities $a_{m1} \ldots$ etc., are defined in reference [9].

Operating on the above set of equations with appropriate differential operators it is shown that the functions $X_m(\eta)$ and $Z_m(\eta)$ may be eliminated from the set, thereby obtaining a single sixth order homogeneous differential equation involving the function $Y_m(\eta)$. Because derivatives of the first, third, and fifth orders are missing from this equation the associated characteristic equation is reduced to a cubic algebraic equation. It is found that for all studies conducted here, the roots are real and are designated as R_1, R_2, and R_3. Following the procedure as described in reference [9], four distinct solution cases are recognized.

They are

$$\text{Case} = 1,\ R_1, R_2, \text{ and } R_3 < 0{\cdot}0; \qquad \text{Case} = 2,\ R_1, R_2 < 0{\cdot}0;\ R_3 > 0{\cdot}0;$$

$$\text{Case} = 3,\ R_1 < 0{\cdot}0;\ R_2 \text{ and } R_3 > 0{\cdot}0; \qquad \text{Case} = 4,\ R_1, R_2 \text{ and } R_3 > 0{\cdot}0. \qquad (19)$$

In fact, for the current studies, only case 3 and case 4 have been encountered for $m > 1$.

One introduces $\alpha = \sqrt{|R_1|}$, $\beta = \sqrt{|R_2|}$, and $\gamma = \sqrt{|R_3|}$, and recognizes that functions $X_m(\eta)$ and $Y_m(\eta)$ must be symmetric with respect to the ξ-axis, while $Z_m(\eta)$ must be

antisymmetric about the same axis. For case 4, one then has

$$Y_m(\eta) = A_m \cosh \alpha\eta + B_m \cosh \beta\eta + C_m \cosh \gamma\eta. \tag{20}$$

It is then shown through the coupling of the set of ordinary differential equations that one may write

$$X_m(\eta) = A_m R_{m1} \cosh \alpha\eta + B_m R_{m2} \cosh \beta\eta + C_m R_{m3} \cosh \gamma\eta \tag{21}$$

and

$$Z_m(\eta) = A_m S_{m1} \sinh \alpha\eta + B_m S_{m2} \sinh \beta\eta + C_m S_{m3} \sinh \gamma\eta. \tag{22}$$

Expressions for $R_{m1}, \ldots, S_{m1}, \ldots$ etc., are obtained following steps described in reference [9]. Expressions for $Y_m(\eta)$, $X_m(\eta)$, etc., for case 3, will differ from the above only in that the first term will involve $\cos \alpha\eta$ instead of $\cosh \alpha\eta$.

The constants A_m, B_m, etc., are evaluated by requiring zero torsional moment and zero edge rotation along the edge, $\eta = 1$. Furthermore, the shear force Q_η, at the edge, $\eta = 1$, must equal the coefficient E_m. Imposing these edge conditions it is readily shown that for case 4 we obtain

$$Y_m(\eta) = (E_m/X3)\{\cosh \alpha\eta + X1 \cosh \beta\eta + X2 \cosh \gamma\eta\}. \tag{23}$$

The functions $X_m(\eta)$ and $Z_m(\eta)$ differ from $Y_m(\eta)$ primarily in that the parameters R_{m1} and S_{m1}, etc., of equations (21) and (22) must be included.

Having performed the above steps the solution for the response of the first building block of Figure 1 is available.

The second, fifth, and sixth building blocks of the figure differ from the first only in that they are driven along a different edge. All of these solutions are therefore readily extracted from that of the first building block. One would normally introduce different subscripts for these other solutions, in order to avoid confusion.

With solutions for the response of the above four building blocks available we direct our attention to the remaining building blocks in the set. These differ from the first four only in that they are driven by distributed harmonic edge rotations and their driven edges are free of transverse shear forces and twisting moments. The driving edge rotation distribution is also represented by the series of equation (1).

The reader will quickly appreciate that the form of solution for these building blocks will be identical to those of the first four transverse-shear driven blocks. The only difference is encountered when one enforces the boundary conditions along the driven edges. As a result, only the quantities $X1$ and $X2$, and the quantities $X1$, $X2$ and $X3$, introduced for the first building block solutions with $m = 1$ and $m > 1$, respectively, will change. One adds the letter P to the corresponding quantities of this latter set of solutions, designating them as $X1P$, $X2P$, etc., for these edge-rotation driven building blocks. One thus has available all of the forced vibration solutions required to conduct the desired free vibration analysis.

2.2. GENERATION OF EIGENVALUE MATRIX

2.2.1. *Plates with lateral elastic support only*

The eigenvalue matrix, which is represented schematically in Figure 2, is generated following established procedures. The corresponding matrix for thin plate studies is described in reference [4].

One begins by enforcing dynamic elastic equilibrium along the edge, $\eta = 1$. Starting with the basic definition of shear force and plate lateral displacement, and moving into the

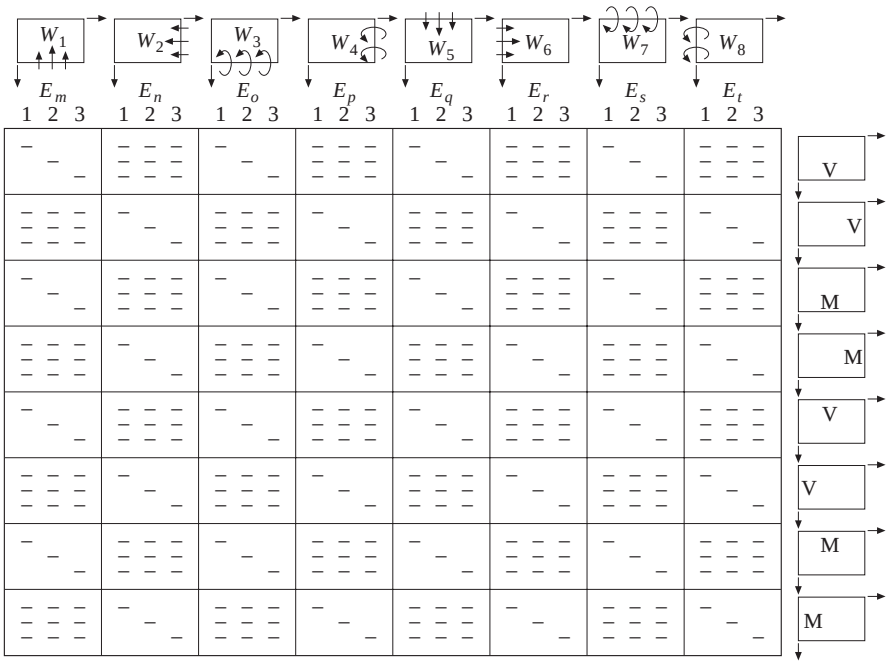

Figure 2. Schematic representation of eigenvalue matrix based on three-term function expansions. Short bars indicate non-zero elements. *M* or *V* on inserts to right indicate edges along which moment or lateral force equilibrium is enforced.

non-dimensional domain it is readily shown that one must enforce the condition

$$Q_\eta + K_{L1} W = 0 \tag{24}$$

along the edge, $\eta = 1$. The plus sign in the above equation must be replaced by a minus sign when dynamic equilibrium is expressed along the edges, $\eta = 0$ and $\xi = 0$. The first set of three homogeneous algebraic equations relating the unknown driving coefficients, based on equation (24), are represented schematically in Figure 2. Following established procedures the displacements W are expanded along the edge in a three-term cosine series. The shear force is already available in such a series. The algebraic equations are obtained by setting the net coefficient of each term in the expansion series representing equation (24), equal to zero.

A second set of equations is obtained by enforcing dynamic equilibrium along the edge, $\xi = 1$, as indicated by the second insert to the right of the figure. The third set of equations is obtained in a similar fashion requiring that the net bending moment along the edge, $\eta = 1$, should vanish. Moving down through Figure 2 it is seen that the complete eigenvalue matrix for the problem is generated. Utilizing K terms in the building block expansions one will have $8K$ unknowns and $8K$ homogeneous equations relating these unknowns.

It will be observed that the matrix has 64 natural segments. Each segment can be referred to by the subscripts I, J. It is expedient to first generate the matrix without including the elastic-support shear forces as observed in equation (24). The matrix is then completed as follows.

(1) Add to the diagonal elements of segments (1, 1) and (2, 2), the quantity 1·0.
(2) Subtract from the diagonal elements of segments (5, 5) and (6, 6), the quantity 1·0.

Physical reasoning permits generation of the eigenvalue matrix to be greatly simplified, in a manner similar to that described in reference [9]. Before making additions and subtractions to diagonal elements as discussed above one can proceed as follows.

(1) Generate those elements only, which lie beneath the first four building blocks of Figure 2.

(2) The remaining segments of the matrix are transferred from those computed above with proper sign changes. It follows immediately that the following segment equalities exist. Segment: $(5, 5) = -(1, 1)K_{L3}/K_{L1}$; $(7, 5) = -(3, 1)$; $(1, 5) = -(5, 1)K_{L1}/K_{L3}$; $(3, 5) = -(7, 1)$; $(5, 7) = -(1, 3)K_{L3}/K_{L1}$; $(7, 7) = -(3, 3)$; $(1, 7) = -(5, 3)K_{L1}/K_{L3}$; $(3, 7) = -(7, 2)$; $(6, 6) = -(2, 2)K_{L4}/K_{L2}$; $(8, 6) = -(4, 2)$; $(2, 6) = -(6, 2)K_{L2}/K_{L4}$; $(4, 6) = -(8, 2)$; $(6, 8) = -(2, 4)K_{L4}/K_{L2}$; $(8, 8) = -(4, 4)$; $(2, 8) = -(6, 4)K_{L2}/K_{L4}$; $(4, 8) = -(8, 4)$.

The following segments are extracted in a similar manner provided one changes signs for the first, third, fifth rows, etc. Segment (2, 5) from (2, 1); (4, 5) from (4, 1); (6, 5) from (6, 1); (8, 5) from (8, 1); (2, 7) from (2, 3); (4, 7) from (4, 3); (6, 7) from (6, 3); (8, 7) from (8, 3); (1, 6) from (1, 2); (3, 6) from (3, 2); (5, 6) from (5, 2); (7, 6) from (7, 2); (1, 8) from (1, 4); (3, 8) from (3, 4); (5, 8) from (5, 4); (7, 8) from (7, 4).

One is now ready to obtain the eigenvalues for any problem of interest by searching for those values of λ^2 which cause the determinant of the associated eigenvalue matrix to vanish. By setting one of the non-zero Fourier driving coefficients equal to unity, solving for the remaining coefficients, and plotting the resulting net displacement, mode shapes are obtained.

2.2.2. *Matrix modifications required to handle edge rotational elasticity*

Fortunately, it is extremely easy to modify the eigenvalue matrix in order to take into account the effects of rotational elastic support along the plate edges. One begins by examining the third set of equations represented schematically in Figure 2. This set pertains to moment equilibrium along the edge, $\eta = 1$. It will be evident that only the third building block in the set contributes toward rotation along this edge. Starting from first principles it is easily shown that edge moment equilibrium is expressed as

$$M_\eta + K_{R1}\psi_\eta = 0. \tag{25}$$

As indicated earlier, the enforced edge rotation, ψ_η, is represented in series form, utilizing the series of equation (1). It follows, therefore, that the only matrix modification required in connection with the above set of equations is described thus. To each diagonal element of segment (3, 3), of the previously existing matrix, one must add the quantity K_{R1}. In a similar fashion one must add to the diagonal elements of segment (4, 4) the quantity K_{R2}, and to the diagonal elements of segments (7, 7) and (8, 8) one must subtract the quantities K_{R3} and K_{R4}, respectively. The eigenvalue matrix now handles problems with both uniform lateral and uniform rotational elastic edge support.

3. PRESENTATION OF COMPUTED RESULTS

3.1. PLATES WITH LATERAL ELASTIC EDGE SUPPORT ONLY

It will be appreciated that numerous verification checks on the analysis can be performed by verifying that computed eigenvalues approach known limits, as the spring stiffness coefficients are allowed to approach their natural limits of zero and infinity. An even more convincing verification test can be performed. It is known that as the thickness-to-length

ratio for the plate is allowed to take on values characteristic of thin plates the results obtained by Mindlin theory must closely approach those obtained by thin plate theory. Results will not coincide exactly, as the thin plate theory does not take plate rotary inertia into consideration and it essentially assumes the plate has infinite stiffness in opposing transverse shear induced deformation. It was demonstrated that all data presented here satisfied the conditions discussed above.

In Figure 3 a semi-logarithmic plot of the first mode eigenvalue versus a dimensionless lateral elastic spring stiffness parameter is presented for a square plate of thickness ratios 0·01 and 0·1. In this, and similar figures, the stiffness parameter covers five decades. These decades have been selected with a view to providing the reader with eigenvalue information over the range of greatest interest. It was found that by plotting eigenvalues against the parameter K_{L1}/ϕ_h^2, instead of K_{L1}, curves for the two ranges of plate thickness ratio, $\phi_h = 0{\cdot}01$ and $\phi_h = 0{\cdot}1$, would fit conveniently on the same figure.

Equal spring stiffness is assigned to each edge of the plate. It will be noted that results for both plate thickness ratios approach zero as the spring stiffness is reduced. As the stiffness parameter is increased the curve associated with the thinner plate approaches $2\pi^2$, the well known eigenvalue for thin simply supported square plates.

Results of Figure 4 differ from those of Figure 3 only in that they pertain to the square plate second mode. Because the plate is square these are in fact repeated eigenvalues and dictate both second and third mode frequencies. Associated with each eigenvalue are two distinct mode shapes, one with a single node line running parallel to the ξ-axis and one with a single node line running parallel to the η-axis; it will be noted that the thinner plate curve approaches the known second mode eigenvalue of $5\pi^2$ based on thin plate theory.

Figure 5 presents eigenvalues for fourth mode vibration of the same plate. The upper eigenvalue limit equals $8\pi^2$ corresponding to the first doubly antisymmetric mode of vibration of the simply supported plate. The lower eigenvalue limit corresponds to the first doubly antisymmetric mode vibration of a completely free square plate and equals 13·489.

Figures 6–9 present similar data related to plates with aspect ratio equal to 1·5, and equal basic elastic edge stiffnesses, k_1, k_2, etc., along each boundary.

Lower eigenvalue limits for the first three modes will, of course, equal zero. Upper limits correspond to eigenvalues for simply supported plates of aspect ratio 1·5. These limits are 14·26, 27·42, and 43·87.

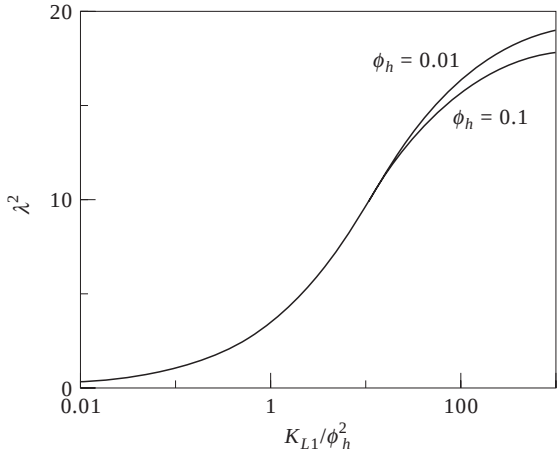

Figure 3. Eigenvalues versus stiffness parameter for square plate first mode vibration: $\phi = 1{\cdot}0$, $K_{L1} = K_{L2} = K_{L3} = K_{L4}$.

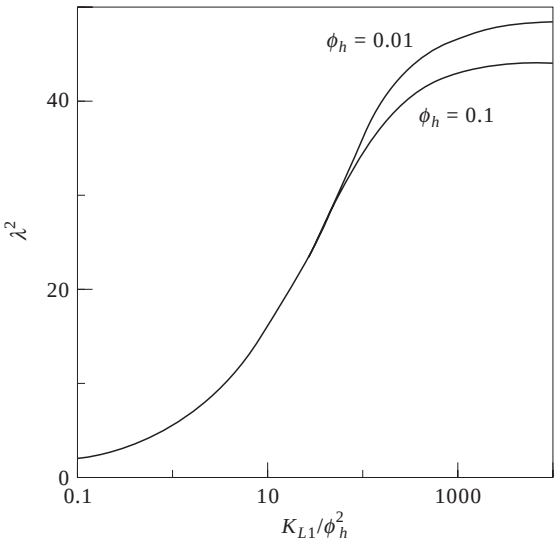

Figure 4. Eigenvalues versus stiffness parameter for square plate second mode vibration: $\phi = 1{\cdot}0$, $K_{L1} = K_{L2} = K_{L3} = K_{L4}$.

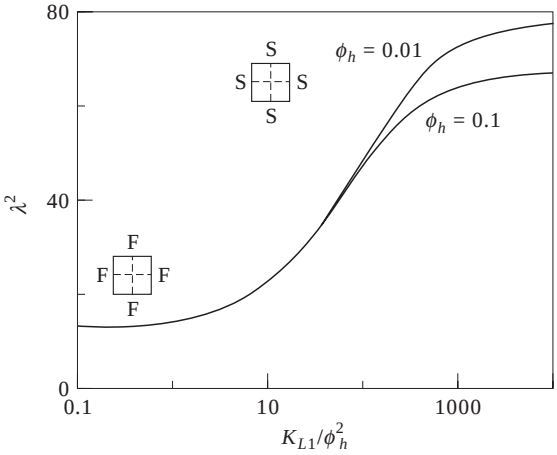

Figure 5. Eigenvalues versus stiffness parameter for square plate fourth mode vibration: $\phi = 1{\cdot}0$, $K_{L1} = K_{L2} = K_{L3} = K_{L4}$. Inserts indicate limiting cases approached.

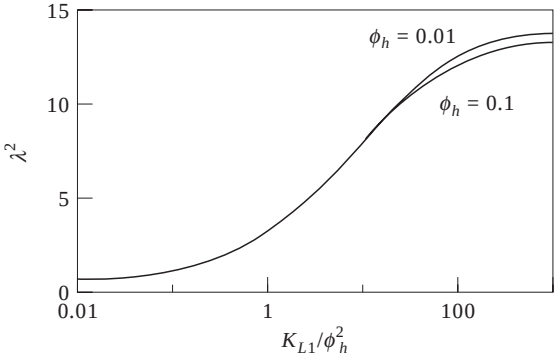

Figure 6. Eigenvalues versus stiffness parameter for rectangular plate first mode vibration: $\phi = 1{\cdot}5$, $k_1 = k_2 = k_3 = k_4$.

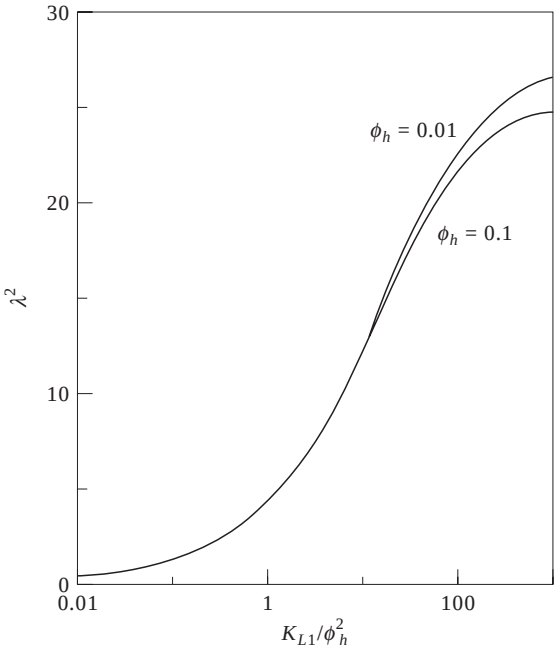

Figure 7. Eigenvalues versus stiffness parameter for rectangular plate second mode vibration: $\phi = 1{\cdot}5$, $k_1 = k_2 = k_3 = k_4$.

The fourth lowest eigenvalue for the plate of apsect ratio 1·5 is plotted in Figure 9. A natural pair of upper and lower eigenvalue limits in this region are provided by the simply supported plate with three half-waves running in the long edge direction, one running in the short edge direction, and a corresponding completely free plate in first mode doubly symmetric mode vibration. Associated eigenvalue limits are 49·35 and 9·412. Another natural pair of limits are provided by the simply supported plate with two half-waves

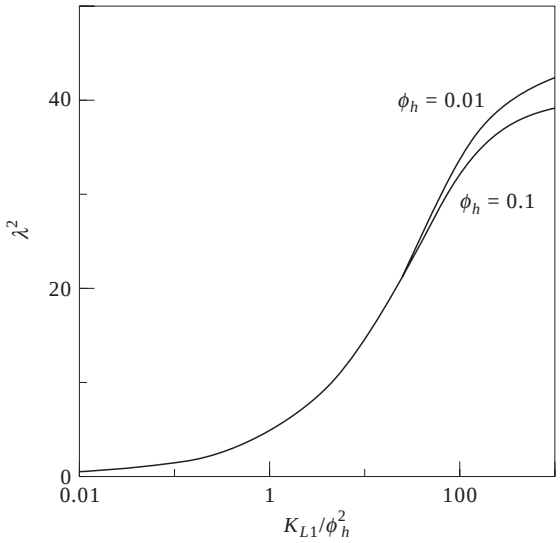

Figure 8. Eigenvalues versus stiffness parameter for rectangular plate third mode vibration: $\phi = 1{\cdot}5$, $k_1 = k_2 = k_3 = k_4$.

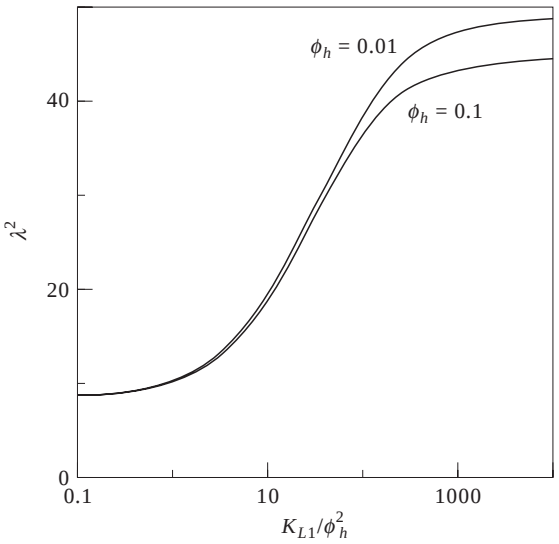

Figure 9. Eigenvalues versus stiffness parameter for rectangular plate fourth mode vibration: $\phi = 1{\cdot}5$, $k_1 = k_2 = k_3 = k_4$.

running along each edge, and the first doubly antisymmetric mode vibration of the completely free plate. Here, associated eigenvalue limits are 57·02 and 8·732.

It is found that the two natural-limit curves discussed above have a cross-over point at about $K_{L1}/\phi_h^2 = 1{\cdot}0$ in Figure 9. That is why the fourth lowest eigenvalue for the problem of Figure 9 has upper and lower eigenvalue limits of 49·35 and 8·732, respectively.

The eigenvalue versus stiffness parameter curves presented so far serve to provide the reader with a general description of the variation of plate eigenvalues with edge stiffness coefficients for a limited number of plate geometries. It will be appreciated that no attempt can be made to provide designers with eigenvalues for all possible plate–edge support configurations. It is also useful, in the author's experience, to provide some eigenvalue information in digital form. This provides other researchers and analysts with valuable results against which their findings can be compared.

A number of highly accurate eigenvalues are tabulated in Tables 1–4. It has been found that convergence is very rapid and four significant digit accuracy can be achieved with only five terms employed in the building block expansion series. Nevertheless, all of the tabulated data have been computed using seven terms in the series. The data covers the first four eigenvalues for each case examined. An attempt has been made to choose the range and invervals in the stiffness parameter in such a way as to cover the eigenvalue range of greatest interest.

3.2. PLATES WITH BOTH LATERAL ELASTIC AND ROTATIONAL ELASTIC EDGE SUPPORT

In Figure 10, results of a typical first mode study involving square plates with lateral and rotational elastic support are presented. The lateral elastic stiffess coefficient is fixed with $K_{L1}/\phi_h^2 = 10\,000$. This is seen to be the highest value utilized in Table 1. The rotational stiffness parameter is allowed to vary over five decades. Each edge of the plate is given equal support.

The eigenvalue curve for the thin plate ($\phi_h = 0{\cdot}01$) begins very close to the known classical eigenvalue for simply supported plates, based on thin plate theory ($2\pi^2$).

TABLE 1

First four eigenvalues for square plates with equal elastic support on all edges: $\phi_h = 0{\cdot}01$

	K_{L1}/ϕ_h^2					
Mode	0·1	1·0	10·0	100·0	1000·0	10 000·0
1	1·171	3·628	9·660	16·33	19·09	19·55
2	1·658	5·220	15·78	35·99	46·96	48·84
3	1·658	5·220	15·78	35·99	46·96	48·84
4	13·26	14·48	23·07	50·17	72·37	77·49

TABLE 2

First four eigenvalues for square plates with equal elastic support on all edges: $\phi_h = 0{\cdot}1$

	K_{L1}/ϕ_h^2					
Mode	0·1	1·0	10·0	100·0	1000·0	10 000·0
1	1·171	3·625	9·593	15·81	17·99	18·30
2	1·650	5·191	15·61	34·47	43·04	44·27
3	1·650	5·191	15·61	34·47	43·04	44·27
4	12·59	13·86	22·55	47·79	64·12	66·98

Furthermore, as the rotational stiffness parameter is increased the curve approaches the classical eigenvalue for fully clamped plates of 35·98.

As expected, the eigenvalue curve for the thicker plate ($\phi_h = 0{\cdot}1$) lies below the first curve. The eigenvalue for the thicker plate in the fully clamped condition is reported by

TABLE 3

First four eigenvalues for rectangular plates with equal basic elastic support on all edges: $\phi = 1{\cdot}5,\ \phi_h = 0{\cdot}01$

	K_{L1}/ϕ_h^2					
Mode	0·1	1·0	10·0	100·0	1000·0	10 000·0
1	1·066	3·244	8·032	12·58	13·96	14·16
2	1·435	4·487	12·70	22·72	26·56	27·18
3	1·588	4·991	14·96	33·65	42·38	43·58
4	8·881	10·35	18·64	38·16	47·47	48·93

TABLE 4

First four eigenvalues for rectangular plates with equal basic elastic support on all edges: $\phi = 1{\cdot}5,\ \phi_h = 0{\cdot}10$

	K_{L1}/ϕ_h^2					
Mode	0·1	1·0	10·0	100·0	1000·0	10 000·0
1	1·066	3·241	7·974	12·21	13·35	13·49
2	1·432	4·473	12·58	21·87	24·89	25·31
3	1·580	4·963	14·80	32·28	39·31	40·18
4	8·524	10·03	18·36	36·36	43·50	44·45

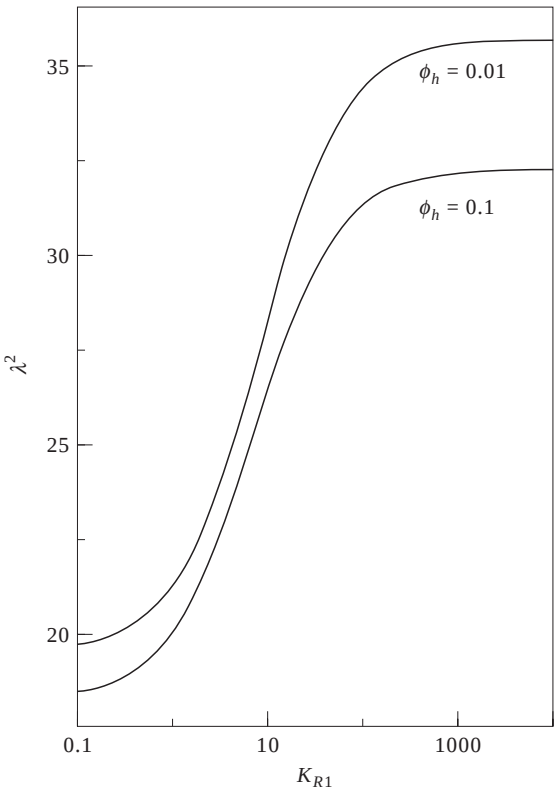

Figure 10. Eigenvalues versus rotational stiffness parameter for square plate first mode vibration: $K_{L1}/\phi_h^2 = K_{L2}/\phi_h^2 = K_{L3}/\phi_h^2 = K_{L4}/\phi_h^2 = 10\,000$, $K_{R1} = K_{R2} = K_{R3} = K_{R4}$.

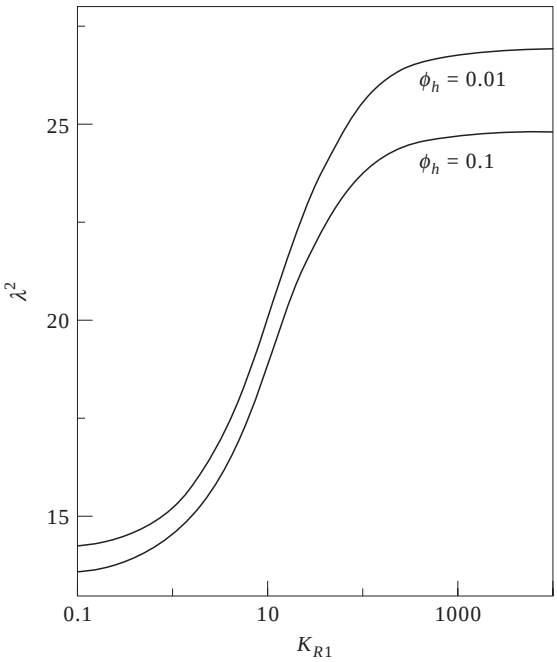

Figure 11. Eigenvalues versus rotational stiffness parameter for rectangular plate first mode vibration: $\phi = 1{\cdot}5$, $K_{L1}/\phi_h^2 = K_{L2}/\phi_h^2 = K_{L3}/\phi_h^2 = K_{L4}/\phi_h^2 = 10\,000$, $k_{R1} = k_{R2} = k_{R3} = k_{R4}$.

TABLE 5

First mode eigenvalues for square plates with equal elastic support on all edges: $K_{L1}/\phi_h^2 = 10\,000$

	K_R					
ϕ_h	0·1	1·0	10·0	100·0	1000·0	10 000·0
0·01	19·75	21·34	28·36	34·46	35·61	35·74
0·1	18·50	20·02	26·35	31·28	32·15	32·24

TABLE 6

Comparison of the results, (*A*) *of Saha et al*. [7], *thin plate results* (*B*) *extracted from reference* [1], *and results of present analysis* (*C*): $\phi_h = 0{\cdot}01$, $\nu = 0{\cdot}3$, $\kappa^2 = 0{\cdot}85$, $(b/a = 1{\cdot}0)$ $(K_{R1} = K_{R2} = K_{R3} = K_{R4},\ K_{L1} - K_{L2} = K_{L3} = K_{L4} = 3000)$

	K_{R1}							
	10^{-7}	10	25	50	100	500	2700	10^7
A	19·43	27·51	30·45	32·00	32·96	33·84	34·04	34·08
B	19·73	27·2	30·2	31·8	33·0	33·8	34·3	35·98
C	19·60	28·46	31·76	33·53	34·63	35·66	35·89	35·94

Yu and Cleghorn [10], as 32·61. Similar results are presented in Figure 11 for plates with an aspect ratio b/a of 1·5. The upper limit based on thin plate theory, i.e., the fully clamped rectangular plate eigenvalue, equals 26·95. The eigenvalue for first mode vibration of the thick plate of aspect ratio 1·5 was reported by Yu and Cleghorn as 24·97. Again, the curves terminate slightly below these upper limits, as expected.

Tabulated eigenvalues as a function of the elastic parameter K_R, with fixed lateral elastic support, are presented in Table 5 for square plates. This data will provide other researchers with digital values against which comparisons can be made.

It is difficult to make comparisons with the findings of Saha *et al*. [7] as almost all of their results are given in the form of curves. Nevertheless, results taken from their Table 5 and results of the present analysis are compared here in Table 6. These results pertain to a thin square plate ($\phi_h = 0{\cdot}01$). Their parameter values were used in the present analysis when computing data entered into this table. The problem studied is essentially that of a thin square plate as it moves from a condition of simple support to a fully clamped condition. This is achieved by letting the rotational stiffness essentially move from zero to infinity. It is seen that at the beginning there is fairly close agreement between the two sets of results. However, as the rotational stiffness coefficient is increased, the results of the present study climb at a slightly higher rate and terminate at a value of 35·94. This is to be expected as the eigenvalue, based on thin plate theory, equals 35·09. Saha *et al*. report a corresponding eigenvalue of 34·08. They also report results taken from reference [11] based entirely on thin plate theory. This latter data was extracted from a plotted curve and cannot be treated with high confidence.

4. SUMMARY AND CONCLUSIONS

The superposition method is shown to provide a powerful and straightforward means of obtaining accurate analytical type solutions to the problem of shear deformable plates

resting on uniform elastic edge supports. Unlike the Rayleigh–Ritz approach, no functions need be selected in advance for representing plate displacement or cross-section rotations. The differential equations are satisfied exactly throughout the domain of the plate and boundary conditions are satisfied to any desired degree of accuracy. Convergence is rapid. All of the known limits for the eigenvalue curves have been approached. Furthermore, results obtained by the Mindlin theory were always found to approach the corresponding results obtained by classical thin plate theory as the thickness-to-length ratio was allowed to decrease.

It is expected that the work reported herein will provide analysts with insight into the character of eigenvalues versus elastic-edge–stiffness curves. Accurate eigenvalues are tabulated in digital form so that they will have reliable data against which they can compare their computed results.

REFERENCES

1. G. B. Warburton and S. L. Edney 1984 *Journal of Sound and Vibration* **95**, 537–552. Vibrations of rectangular plates with elastically restrained edges.
2. C. S. Kim, P. G. Young and S. M. Dickinson 1990 *Journal of Sound and Vibration* **143**, 379–394. On the flexural vibration of rectangular plates approached by using simple polynomials in the Rayleigh–Ritz method.
3. D. J. Gorman 1989 *Journal of Applied Mechanics* **56**, 893–899. A comprehensive study of the free vibration of rectangular plates resting on symmetrically distributed uniform elastic edge supports.
4. D. J. Gorman 1990 *Journal of Sound and Vibration* **139**, 325–335. A general solution for the free vibration of rectangular plates resting on uniform elastic edge support.
5. D. J. Gorman 1993 *Journal of Sound and Vibration* **163**, 1–12. Free vibration analysis of rectangular plates with step-wise discontinuities in rotational stiffness along the edges.
6. D. J. Gorman 1994 *Journal of Sound and Vibration* **174**, 451–459. A general solution for the free vibration of rectangular plates with arbitrarily distributed lateral and rotational elastic edge support.
7. K. N. Saha, R. C. Kar and P. K. Datta *Journal of Sound and Vibration* **192**, 885–904. Free vibration analysis of rectangualr Mindlin plates with elastic restraints uniformly distributed along the edges.
8. S. D. Yu and W. L. Cleghorn 1992 *Proceedings of a Symposium on Engineering Applications of Mechanics*, *University of Regina*, *Regina Saskatchewan*, 11–13 *May*, 226–230. Accurate free vibration analysis of clamped Mindlin plates using the method of superposition.
9. D. J. Gorman 1996 *Journal of Sound and Vibration* **189**, 341–353. Accurate free vibration analysis of the completely free rectangular Mindlin plate.
10. S. D. Yu and W. L. Cleghorn 1993 93-*CSME*-14, *E.I.C. Accession No* 2331, **17**, 2. Accurate free vibration analysis of clamped Mindlin plates using the method of superposition.
11. D. J. Gorman 1990 *Journal of Sound and Vibration* **139**, 325–335. A general solution for the free vibration of rectangular plates resting on uniform elastic edge supports.

APPENDIX: LIST OF SYMBOLS

a, b	plate edge dimensions
D	$= Eh^3/(12(1-\nu^2))$, plate flexural rigidity
E	Young's modulus of plate material
G	modulus of elasticity in shear of plate material
h	plate thickness
$k_1, k_2, \ldots$	basic lateral spring stiffness along plate edge; subscript 1 indicates edge, $\eta = 1$; 2, 3, 4, indicate edges moving counter-clockwise from 1
$K_{L1}, K_{L2}, \ldots$	dimensionless lateral elastic edge coefficients, $= k_1 aw/\kappa^2 Gh$, $k_2 aw/\kappa^2 Gh$, etc.
$k_{R1}, k_{R2}, \ldots$	basic rotational spring stiffness along plate edges
$K_{R1}, K_{R2}, \ldots$	dimensionless rotational elastic edge coefficients, $= k_{R1} b/D$, $k_{R2} a/D$, $k_{R3} b/D$, $k_{R4} a/D$.
M_ξ, M_η	dimensionless bending moments associated with ξ and η directions, respectively

$M_{\xi\eta}$	dimensionless twisting moment
Q_ξ, Q_η	dimensionless shear forces associated with ξ and η directions, respectively
W	plate lateral displacement divided by side length a
ξ, η	distances along plate co-ordinate axes divided by side lengths a, and b, respectively
κ^2	Mindlin shear factor = 0·8601
v	Poisson ratio of plate material = 0·333
v_1	$=(1-v)/2$
v_2	$=(1+v)/2$
v_3	$=6\kappa^2(1-v)$
ϕ	plate aspect ratio = b/a
ϕ_h	plate thickness ratio = h/a
ψ_ξ, ψ_η	plate cross-section rotations associated with ξ and η directions, respectively
ω	circular frequency of plate vibration
λ^2	$=\omega a^2\sqrt{\rho/D}$, free vibration eigenvalue
ρ	mass of plate per unit area